LANGLEY GRANT
IN-24-CR
97284
38P.

WASHINGTON UNIVERSITY
DEPARTMENT OF PHYSICS
LABORATORY FOR ULTRASONICS
St. Louis, Missouri 63130

"Quantitative Non-Destructive Evaluation of Porous Composite Materials Based on Ultrasonic Wave Propagation"

Semiannual Progress Report: March 15, 1987 - September 14, 1987

NASA Grant Number: NSG-1601

Principal Investigator:

Dr. James G. Miller

Professor of Physics

The NASA Technical Officer for this grant is:

Dr. Joseph S. Heyman

NASA Langley Research Center

Hampton, Virginia

(NASA-CR-181275) QUANTITATIVE NON-DESTRUCTIVE EVALUATION OF POROUS COMPOSITE MATERIALS BASED ON ULTRASONIC WAVE PROPAGATION Semiannual Progress Report, 15 Mar. - 14 Sep. 1987 (Washington Univ.) 38 G3/24 N87-29601 Unclas 0097284

I. INTRODUCTION

This progress report summarizes our continuing research into the quantitative nondestructive evaluation of composite materials. In previous reports we have described investigations of impact damage in graphite-epoxy composites. In this report we shift our emphasis somewhat and describe investigations we have carried out to characterize porosity in composite media using ultrasonic waves. These investigations are described in Section II. Previous reports have also described our investigations of local approximations to the Kramers-Kronig relations. In Section III of this Progress Report we present a derivation of these relations and show that they may also be applicable to systems that could conceivably exhibit considerable dispersion such as composite laminates containing porosity.

II CHARACTERIZATION OF POROSITY IN COMPOSITE LAMINATES

IIa. INTRODUCTION

The detrimental effects of porosity on material strength are well known. The work of Rose, Hsu, and Adler provides a means of estimating the volume fraction of pores and the average pore radius in isotropic elastic media from the value of frequency at which the attenuation coefficient becomes frequency independent and the magnitude of the attenuation coefficient at that plateau.[1] Quantitative results for the isotropic case depend on numerical factors obtained by Gubernatis et al. which are functions of the ratio of the transverse to longitudinal sound velocities.[2] Adler, Rose, and, Mobley have tested these theories by making measurements of attenuation covering a frequency range that extended well into the frequency independent plateau.[3] Recent investigations suggest the feasibility of applying these methods to estimate the volume fraction of porosity in composite laminates.[4-10] The experimental results of these investigators suggest that the theoretical results obtained by Rose et al. are qualitatively correct even though some of the features of wave propagation in layered, anisotropic media are not explicitly incorporated into the scattering model.

In this report, we consider an approach to deal with the case of anisotropic media, in which the magnitude of the attenuation may preclude making measurements at sufficiently high frequencies to reach the plateau region. Approaches to materials characterization based on the frequency dependence (slope) of attenuation are widely

employed in medical ultrasonics.[11] A well-known experimental result for frequencies lower than that corresponding to the plateau (i.e., $f < f_{high}$) but above the Rayleigh region ($f > f_{low}$) is that the attenuation coefficient exhibits an approximately linear increase with frequency over a range from f_{low} to f_{high}. Typically the useful bandwidth of the measurement is substantially smaller than this range and falls at an unknown location between these limits. Fortunately, the expression for the attenuation coefficient contains numerical factors which depend only weakly on the ratio of f_{high} to f_{low}, varying only by a factor of 3 for the ratio of f_{high} to f_{low} ranging from 10 to 1 to 10,000 to 1. In the case of composites with complex lay-ups for which a detailed theory that describes the effects of porosity on attenuation may not be available, empirical knowledge of these numerical factors obtained from laminates of known porosity might provide an approach for estimating the porosity from ultrasonic measurements of similar composites.

To evaluate this approach we measured the slope of attenuation as a function of frequency in a set of 5 glass-fiber/epoxy-matrix test specimens with simulated porosity (glass spheres) ranging from 0% to 12% (volume fraction) and a set of 5 uniaxial graphite-fiber/epoxy-matrix specimens with simulated porosity (glass spheres) ranging from 1% to 8%. Good correlation was obtained between the measured slopes and porosity in each case, suggesting that semi-quantitative estimates of porosity can be achieved without measurements in the plateau region and without a quantitative theory.

IIb. EXPERIMENTAL METHODS

1) SAMPLE PREPARATION

The effects of porosity were simulated using solid glass beads, 75 to 150 microns in diameter, in 16 ply uniaxial graphite-fiber/epoxy-matrix composites. These composites were fabricated using 5208-T300 prepreg tape. Measured amounts of glass beads were introduced between the 12th and 13th layers during the lay-up of a 12 by 16 inch composite. The beads were dusted onto circular regions 2 inches in diameter at sites on a square grid with centers 4 inches apart. The sample was autoclaved and cured in an oven using a standard cure protocol. The 12 by 16 inch sample was cut into smaller samples (approximately 3.75" by 3.75") so that each contained a single zone of "porosity" with a volume fraction of 1%, 2%, 4%, 6%, or 8%.

2) MEASUREMENT METHODS

The signal loss was measured in transmission mode with a specimen placed in the overlapping focal zones of a matched pair of 25 MHz center frequency, 0.25 inch

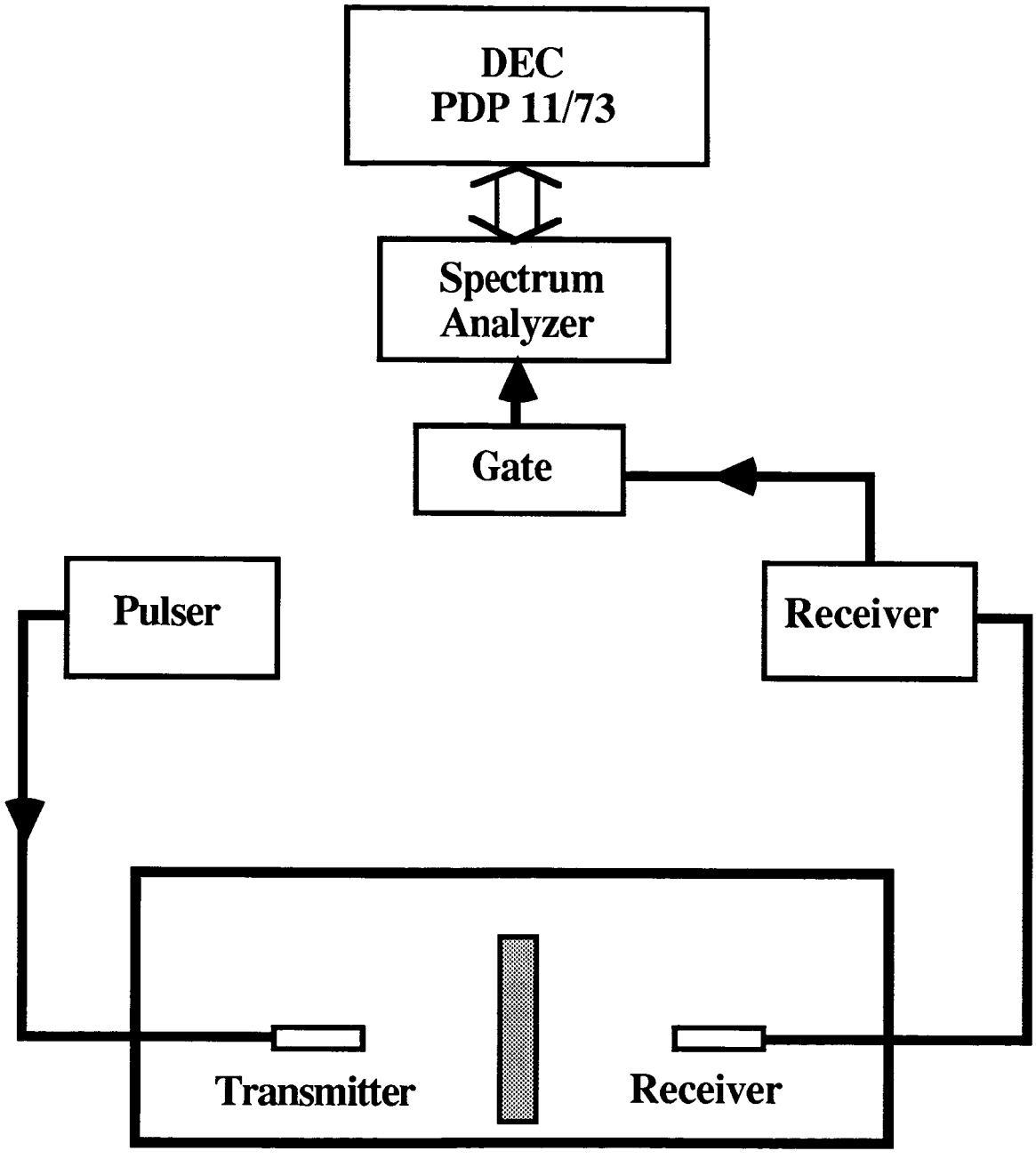

Figure 1. Block diagram of the transmission mode acquisition system used for measurements of attenuation in porous graphite/epoxy composites.

diameter, 1 inch focal length transducers. Each sample was scanned on a 21 by 21 grid in 1 mm steps and the acquired frequency spectra averaged to reduce the effects of spatial variations of "porosity" within the samples.

The measurement system used for data acquisition is illustrated schematically in Fig. (1). The transmitting and receiving transducers were oriented so that the insonifying beam was perpendicular to the surfaces of the sample and were aligned by viewing the received signal on a spectrum analyzer. A Metrotek MP215 wideband pulser was used to drive the transmitting transducer. The output of a MR106 wideband receiver was routed to a stepless gate and the 1.5 μsec gated signal was subsequently used as the input to the spectrum analyzer. A DEC PDP 11/73 running the UNIX operating system was used to control the motor driven apparatus on a C-scan tank (in which the samples were placed for data acquisition) as well as to acquire the data from the spectrum analyzer for storage and subsequent analysis.

IIc. DATA ANALYSIS

The signal loss through the composite laminate was obtained by normalizing the averaged frequency spectrum with a calibration spectrum obtained from a water-only-path trace,

$$Signal\ Loss = log\,[calibration\ spectrum] - log\,[sample\ spectrum]\,. \qquad (1)$$

This method of log spectral subtraction is performed to deconvolve effects arising from the electromechanical response of the transducers and front-end electronics from the sample spectrum. The normalized data were analyzed by performing a Taylor expansion around the center frequency $\bar{f}$ of the useful bandwidth,

$$Signal\ loss \approx K_0 + K_1 \times (f - \bar{f}\,) \qquad (2)$$

where K_0 is an estimate of the average signal loss over the useful bandwidth, and K_1 is the rate of change of the signal loss with respect to frequency. This procedure is illustrated in Fig. (2) where the signal loss of a typical spectrum is plotted as a function of frequency along with the appropriate Taylor expansion. The usable bandwidth of this system was 3 to 12 MHz, where the upper limit was due to the increasing attenuation coefficient as function of frequency exhibited by the composite laminates.

IIc. METHOD VALIDATION

In order to validate our methods, measurements were made on a set of 5 glass-fiber/epoxy-matrix composites containing controlled amounts of simulated "porosity" (0%, 1%, 3%, 6%, or 12% volume fraction). The glass fibers were approximately 12 μm

Figure Two

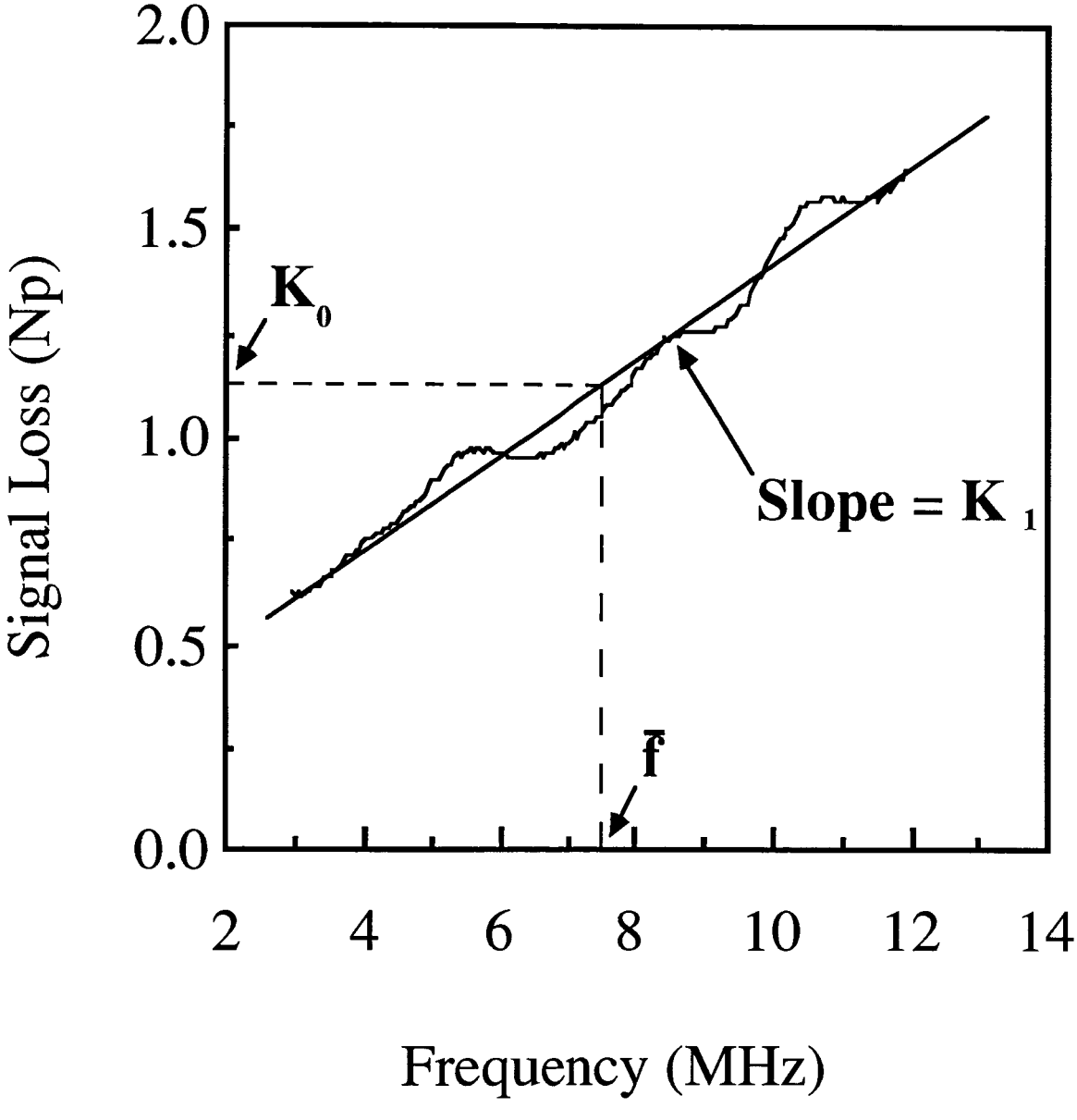

Figure 2. Plot displaying a typical signal loss and the corresponding Taylor expansion given by Eq. (2).

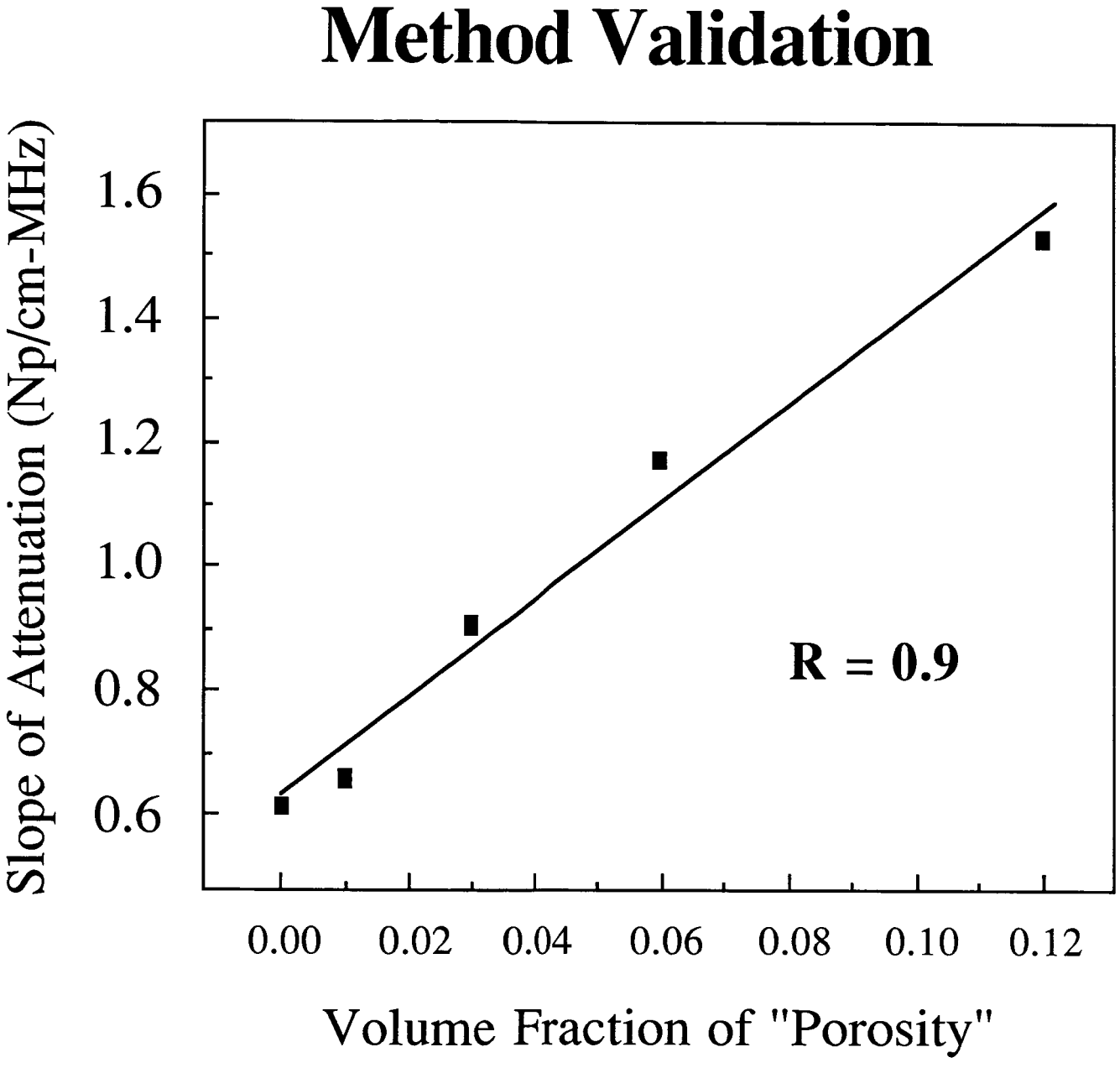

Figure 3. Validation of the proposed method. Preliminary experiments were performed on glass-fiber/epoxy-matrix composites with controlled amounts of "porosity" (simulated by solid glass inclusions).

in diameter and four to five centimeters in length. The fibers ($\rho = 2.43 \pm 0.09\ gm/cm^3$) were layed-up by hand in an epoxy resin matrix ($\rho = 1.10 \pm 0.01\ gm/cm^3$). Porosity was simulated by the random inclusion of solid lead-glass spheres ($\rho = 2.47 \pm 0.04\ gm/cm^3$) drawn from a distribution with radii ranging between 37 μm and 75 μm. These test samples were fabricated with a fiber volume fraction of approximately 8%. One sample was fabricated without glass beads in order to serve as a control.

The results of this control study are presented in Fig. (3) in which the slope of the attenuation is plotted versus volume fraction of "porosity". The correlation coefficient obtained by performing a linear regression between slope of attenuation and the volume fraction of "porosity" is 0.9, suggesting the potential of the method.

IId. THEORY

Rose has derived an expression for the concentration of hollow spheres embedded in an elastic medium,

$$Conc. = \frac{4}{3A_2\pi} \int_0^\infty \frac{\alpha(k)}{k^2}\, dk \tag{3}$$

where $\alpha(k)$ is the excess attenuation due to the scattering of sound waves by the pores.[12] That is, $\alpha(k)$ represents the increase in the attenuation produced by the addition of hollow spherical pores to the material above that due to the attenuation from the elastic background medium. We consider the case in which the excess attenuation due to the presence of porosity can be approximated by

$$\alpha(f) = (excess\ attenuation) = (excess\ K_1) \times \begin{cases} \frac{1}{f_{low}^3} f^4 & f < f_{low} \\ f & f_{low} < f < f_{high} \\ f_{high} & f > f_{high}. \end{cases} \tag{4}$$

as illustrated in Fig. (4).

This model implies an f^4 dependent Rayleigh scattering in the low frequency region, and a frequency independent geometrical scattering in the high frequency region. The approximately linear dependence on frequency in the intermediate region is well supported from experimental measurements performed on composite laminates. Because of the finite usable bandwidth of the experimental apparatus, both f_{high} and f_{low} are usually unknown. Nevertheless, the relationship between the volume concentration of porosity and excess K_1 is only weakly dependent upon the ratio of f_{high} to f_{low}.

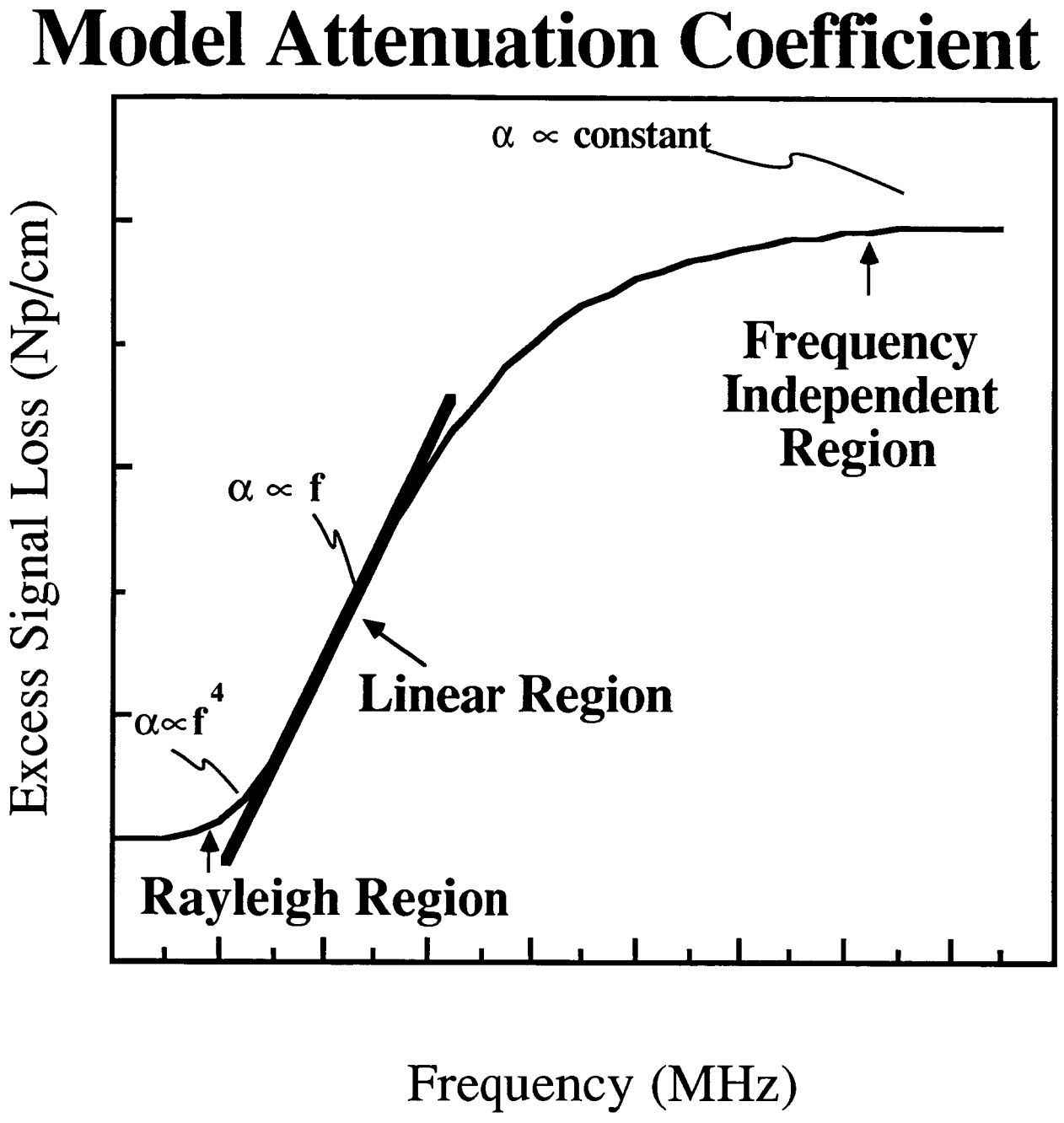

Figure 4. Illustration of the phenomenological model.

Figure 5

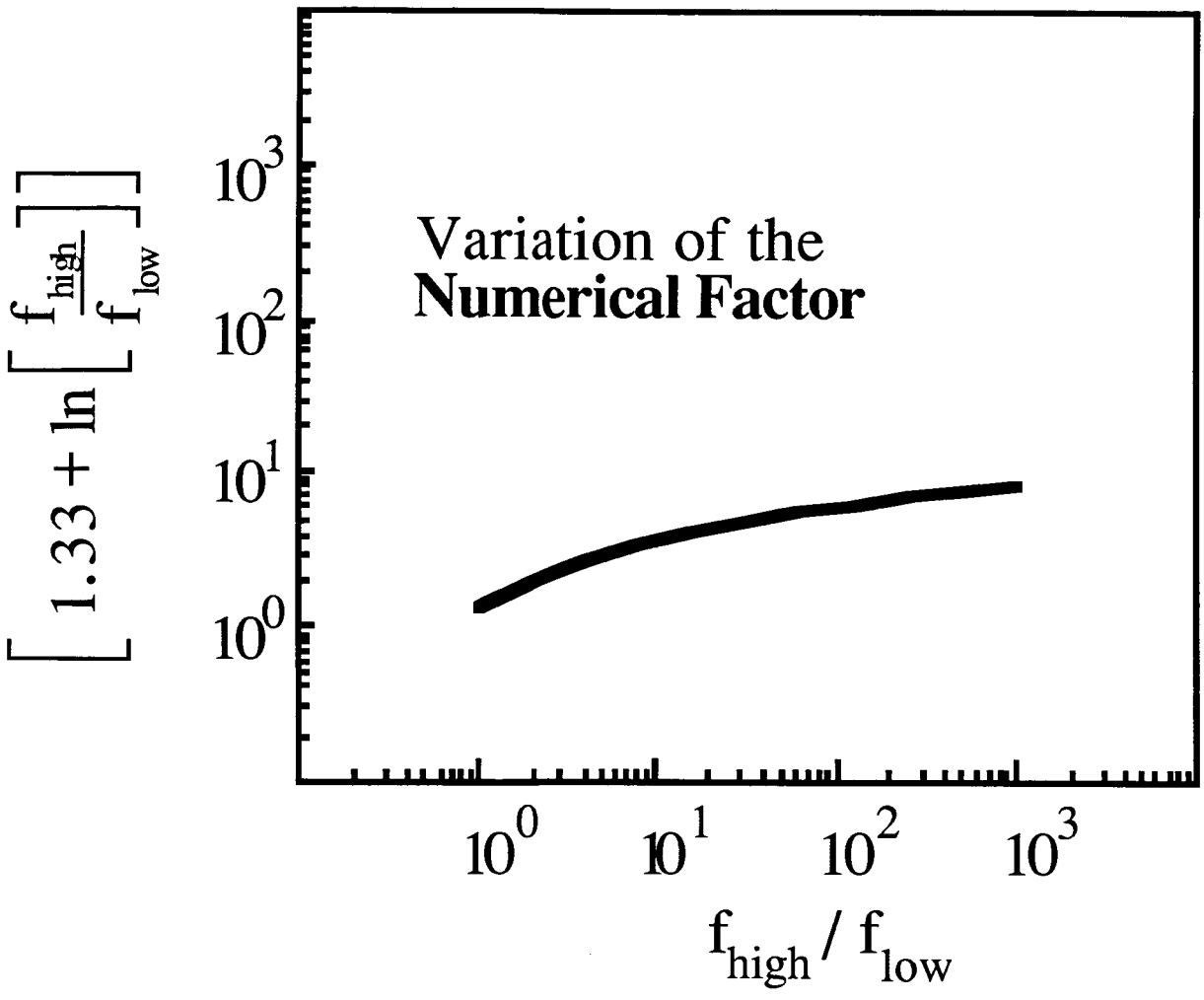

Figure 5. Plot illustrating the slow variation of the **Numerical Factor** as a function of the ratio of f_{high} to f_{low}

Inserting Eq.(4) into Eq.(3) leads to

$$Conc. = \frac{4}{3A_2\pi} \times \frac{V}{2\pi} \times (excess\ K_1) \times \left\{ \frac{1}{f_{low}{}^3} \int_0^{f_{low}} f^2\, df + \int_{f_{low}}^{f_{high}} \frac{df}{f} + \int_{f_{high}}^{\infty} \frac{f_{high}\, df}{f^2} \right\} \quad (5)$$

or

$$Conc. = (excess\ K_1) \times \frac{4}{3A_2\pi} \times \frac{V}{2\pi} \times \left[\frac{1}{3} + \ln\left[\frac{f_{high}}{f_{low}} \right] + 1 \right] . \quad (6)$$

It is convenient to express this result as

$$Conc. = (excess\ K_1) \times Velocity \times [\textbf{Numerical Factor}] , \quad (7)$$

where

$$\textbf{Numerical Factor} \equiv \frac{4}{3A_2\pi} \times \frac{1}{2\pi} \times \left[\frac{1}{3} + \ln\left[\frac{f_{high}}{f_{low}} \right] + 1 \right] . \quad (8)$$

The **Numerical Factor** is a slowly varying function of the ratio f_{high}/f_{low} over several decades, as illustrated in Fig. (5). Because f_{high} and f_{low} are rarely known, this slow variation is the basis for the predictive usefulness of the model.

IIe. RESULTS and CONCLUSIONS

The results obtained for the graphite-fiber/epoxy-matrix specimens are displayed in Fig. (6). The scatter plot displays the resultant slope of attenuation (from the spatially-averaged normalized spectrum) for each of the five samples versus the volume fraction of "porosity" for that sample. The slope of attenuation correlates well (r = 0.9) with concentration of "porosity". An examination of Equation(7) indicates that the value of the **Numerical Factor** for the composite laminates under investigation can be determined from the slope of the "Slope of Attenuation" versus the "Volume Fraction of Porosity" correlation plot,

$$\textbf{Numerical Factor} = \left[Velocity \times Slope\ of \left\{ \begin{array}{c} Slope\ of\ Attenuation \\ versus \\ Vol.\ Fraction\ of\ Porosity \end{array} \right\} \right]^{-1} . \quad (9)$$

For the glass-fiber/epoxy-matrix composites used to validate our procedure the value of the **Numerical Factor** was found to be ≈ 0.5 (using a velocity of 0.25 cm/μsec) and for the graphite-fiber/epoxy-matrix composites studied the value for the **Numerical Factor** was found to be ≈ 2 (using a velocity of 0.30 cm/μsec). The good agreement between the

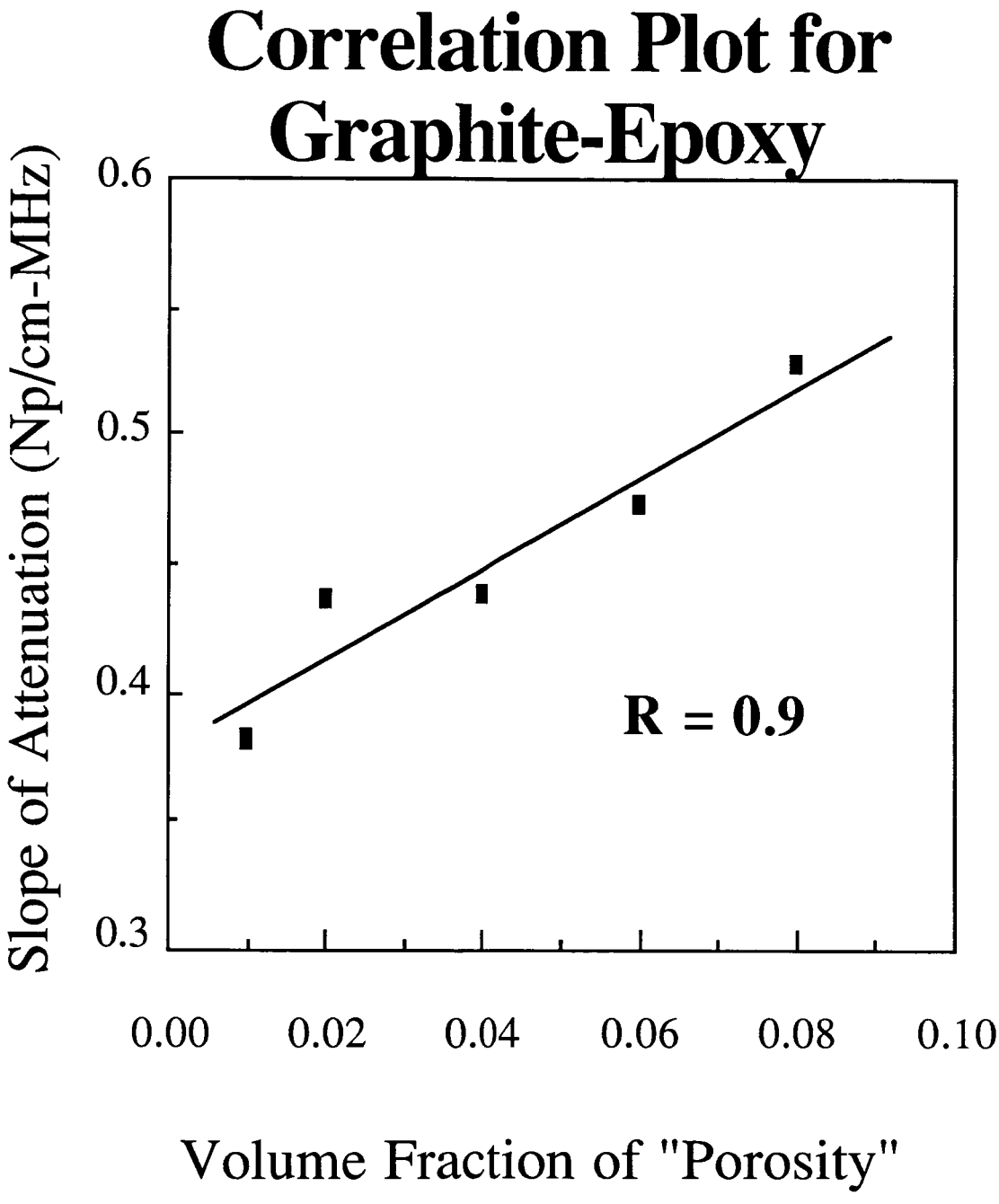

Figure 6. Correlation plot for measurements on graphite-fiber/epoxy-matrix composites.

experimental data and the phenomenological model suggests that this approach may be useful in estimating concentrations of porosity in composite laminates.

III KRAMERS-KRONIG RELATIONSHIPS

IIIa. INTRODUCTION

Previous reports from this Laboratory have focused on local approximations to the following Kramers-Kronig relationships

$$K_1(\omega)-K_1(\infty) = \frac{2}{\pi}\int_0^\infty \frac{\omega' K_2(\omega')}{\omega'^2-\omega^2}\,d\omega' \tag{10}$$

$$K_2(\omega) = -\frac{2\omega}{\pi}\int_0^\infty \frac{K_1(\omega')-K_1(\infty)}{\omega'^2-\omega^2}\,d\omega' \tag{11}$$

where $K_1(\omega)$ and $K_2(\omega)$ are the real and imaginary parts, respectively, of the dynamic compressibility $K(\omega)$. Tests of several approximations to these exact relations have been reported on previously (every progress report from the 9/15/85 to 3/14/86 report to this one). In the last proposal we indicated our intention to provide a derivation of the local approximation to Eq. (10) on which our previous investigations were based. The next two portions of this report, Sections IIIb and IIIc, present such a derivation. They also demonstrate that the local approximation we have tested may be applicable in systems exhibiting considerable dispersion such as carbon-carbon composites.

IIIb. DERIVATION OF TWO LOCAL APPROXIMATIONS

The nonlocal character of Equations (10) and (11) limits their usefulness. Frequency domain data extending over the range from 0 to ∞ is never available experimentally due to the limited bandwidth of any measurement system. Computable approximations to Eqs. (10) and (11) are needed. The purpose of this Section is to derive a local approximation to the Kramers-Kronig relations. The approximation derived here is not the only local approximation to these equations which is possible. In fact, most of the common Hilbert transform pairs do not satisfy the approximation that will be derived here.[13]

We will present a derivation of a local approximation in a very general setting. In order to do this we will first rewrite the Kramers-Kronig relations in a more general notation

$$B(\omega) = \frac{2\omega}{\pi}\int_0^\infty \frac{A(u)-A(\omega)}{u^2-\omega^2}\,du\ . \tag{12}$$

where $A(\omega)$ and $B(\omega)$ are the real and imaginary parts respectively of a general frequency response function $\Theta(\omega)$. The dynamic compressibility given above $K(\omega)$ is just one of many choices we could have made for the frequency response function. In fact, many researchers have taken as their starting point the acoustic index of refraction and then proceeded from the Kramers-Kronig relations relation between the real and imaginary parts of this quantity. This result is essentially equivalent to the approach we have taken as long as we assume that the attenuation coefficient is greater than zero for all frequencies but zero and ∞ which seems reasonable. (This claim will be substantiated below, in Section IIIc.2.) The first step in the approximation scheme is make the change of variables

$$x \equiv u/\omega . \tag{13}$$

With this change of variables the integral becomes

$$B(\omega) = \frac{2}{\pi}\int_0^{\infty} \frac{A(\omega x)-A(\omega)}{x^2-1}dx , \tag{14}$$

where the integration variable is now dimensionless. Now the first in a series of approximations is made by writing

$$B(\omega) \approx \frac{2}{\pi}\int_{1-\rho/\omega}^{1+\rho/\omega} \frac{A(\omega x)-A(\omega)}{x^2-1}dx . \tag{15}$$

where ρ is the distance between ω and the nearest singularity of $A(u)$ in the complex u plane. If it happens that $\rho > \omega$ then the appropriate approximation is

$$B(\omega) \approx \frac{2}{\pi}\int_0^{1+\rho/\omega} \frac{A(\omega x)-A(\omega)}{x^2-1}dx . \tag{16}$$

Before proceeding it is worth noting that Eq. (15) constitutes an example of the finite Hilbert transform. As such the exact of the approximate equation is available.[14] However, this approach is not pursued here. Making the approximation in Eq. (15) involves neglecting the tails of the integral. The first term neglected is

$$\frac{2}{\pi}\int_0^{1-\rho/\omega} \frac{A(\omega x)-A(\omega)}{x^2-1}dx \tag{17}$$

which has, due to Assumption 1b), an absolute value less than

$$\frac{2M}{\pi}\int_0^{1-\rho/\omega} \frac{1}{x^2-1}dx . \tag{18}$$

Thus the absolute value of the first tail is less than

$$\frac{M}{\pi}\ln\left[\frac{\rho/\omega}{2-\rho/\omega}\right] \tag{19}$$

for $\rho \le \omega$, and is equal to 0 for $\rho \ge \omega$. The other tail is

$$\frac{2}{\pi}\int_{1+\rho/\omega}^{\infty}\frac{A(\omega x)-A(\omega)}{x^2-1}dx\ , \tag{20}$$

which has an absolute value that is less than

$$\frac{2M}{\pi}\int_{1+\rho/\omega}^{\infty}\frac{1}{x^2-1}dx. \tag{21}$$

Making the further change of variables $z = x-1$ leads to

$$\frac{2M}{\pi}\int_{1+\rho/\omega}^{\infty}\frac{1}{x^2-1}dx = \frac{2M}{\pi}\int_{\rho/\omega}^{\infty}\frac{1}{z^2+2z}dz \le \frac{2M}{\pi}\int_{\rho/\omega}^{\infty}\frac{1}{z^2}dz \tag{22}$$

Hence,

$$\frac{2}{\pi}\int_{1+\rho/\omega}^{\infty}\frac{A(\omega x)-A(\omega)}{x^2-1}dx \le \frac{2M\omega}{\pi\rho} \tag{23}$$

A review of the error bounds that have been established so far indicates that in the case where $\omega \ll \rho$ these errors will decrease to zero. (Under some circumstances, it is also possible that the term that has been retained may be decreasing to zero at the same rate, in which case the approximation will fail.)

The next step in the approximation scheme is to expand $A(u)$ in an infinite series, using Burmann's series expansion.[15] The expansion is given in the following theorem:

Burmann's Theorem:

Let $\psi(z)$ be a function defined by the equation

$$\psi(z) = \frac{z-a}{\phi(z)-\phi(a)}, \tag{24}$$

where $\phi(z)$ is analytic in a circle centered at $z=a$. Then any function $f(z)$ analytic in the same circle centered at a can be expanded in the form

$$f(z) = f(a) + \sum_{m=1}^{n-1}\frac{\{\phi(z)-\phi(a)\}^m}{m!}\frac{d^{m-1}}{da^{m-1}}[f'(a)\{\psi(a)\}^m] + R_n \tag{25}$$

where

$$R_n = \frac{1}{2\pi i}\int_z^a d\xi\int_\gamma dt\left[\frac{\phi(\xi)-\phi(a)}{\phi(t)-\phi(a)}\right]^{n-1}\frac{f'(t)\phi'(\xi)}{\phi(t)-\phi(\xi)}, \tag{26}$$

and γ is a contour in the t-plane, enclosing the points a and z and such that, if ζ be any point inside it, the equation $\phi(t) = \phi(\zeta)$ has no roots on or inside the contour except a simple root $t = \zeta$.

Of course the choice of ϕ is completely arbitrary up to the conditions imposed by the theorem. It is this arbitrariness which makes it possible to derive many different local approximations to the Kramers-Kronig relations. ϕ should be chosen so that the first few terms of the series provide a good estimate of $A(u)$ over the frequency range of interest. This choice is extremely important to approximations based on experimental data where the calculation of even the first derivative is often unreliable due to noise.

If the function $A(\omega)$ is a slowly varying function of ω then it would seem reasonable to expand $A(\omega)$ in terms of a function ϕ which is also varying. In this case one choice for ϕ is

$$\phi(u) = \ln(u/\omega) \tag{27}$$

where the argument of ϕ has been chosen to be a dimensionless function of ω. With this choice of ϕ, ψ becomes

$$\psi(\omega) = \lim_{u\to\omega}\psi(u) = \lim_{u\to\omega}\frac{u-\omega}{\ln(u/\omega)-0} = \lim_{u\to\omega}\frac{1}{\frac{1}{u}} = \omega\,. \tag{28}$$

Inserting this into Burmann's expansion leads to the following series representation for $A(u)$

$$A(u) = A(\omega) + \sum_{m=1}^{\infty}\frac{\{\ln(u/\omega)\}^m}{m!}\frac{d^{m-1}}{d\omega^{m-1}}[A'(\omega)\omega^m] \tag{29}$$

where a prime denotes differentiation with respect to ω, since the expansion of $A(u)$ was carried out in the complex u-plane which contains ω. Using this sum in Eq. (15) leads to

$$B(\omega) \approx \frac{2}{\pi}\int_{1-\rho/\omega}^{1+\rho/\omega}\frac{1}{x^2-1}\sum_{m=1}^{\infty}\frac{\{\ln(x)\}^m}{m!}\frac{d^{m-1}}{d\omega^{m-1}}[A'(\omega)\omega^m]dx\,. \tag{30}$$

Assuming that the series in Eq. (29) is uniformly convergent and recalling that the integral appearing in Eq. (30) may be thought of as a principal value integral, we see that it is possible to bring the summation outside of the integral to produce

$$B(\omega) \approx \frac{2}{\pi}\sum_{m=1}^{\infty}\frac{1}{m!}\frac{d^{m-1}}{d\omega^{m-1}}[A'(\omega)\omega^m]\int_{1-\rho/\omega}^{1+\rho/\omega}\frac{\{\ln(x)\}^m}{x^2-1}dx \tag{31}$$

It is still, however, appropriate to think of the integral in Eq. (10) and, hence, Eq. (30) as

a principal value integral. With this restriction the singularity at $x = 1$ is excluded from the integration range and thus if Burmann's series, Eq. (29), is uniformly convergent over the range of integration then so is the series obtained by dividing Eq. (29) by $1/(x^2 - 1)$.) The next step is to further approximate each of these integrals by moving the lower bound of integration back to 0 and moving the upper bound out to ∞. It is an easy matter to evaluate the error introduced by taking the upper bound of integration out to ∞. Error estimates are obtained by evaluation of

$$\int_{1+\rho/\omega}^{\infty} \frac{\{\ln(x)\}^m}{x^2 - 1} dx \tag{32}$$

which goes to zero as $\rho \to \infty$ for fixed ω. Estimation of the error introduced by taking the lower bound of integration back to 0 is harder to obtain. These error estimates would involve evaluation of integrals like

$$\int_{0}^{1-\rho/\omega} \frac{\{\ln(x)\}^m}{x^2 - 1} dx \tag{33}$$

all of which have a singularity at the lower bound of integration. However, if $\omega \ll \rho$ then it will not even be necessary to evaluate these integrals since the integration range already extends to 0 in that case. Of course, all integrals must be taken as principal value integrals in order to exclude the singularity at $x = 0$ from the range of integration. Furthermore, it is apparent that if the frequency response function is getting small around ω then the errors introduced by moving the bounds of integration as just discussed may cause the approximation to fail.

Having the range of integration as described above, we see that the expression for $B(\omega)$ is now

$$B(\omega) \approx \frac{2}{\pi} \sum_{m=1}^{\infty} \frac{1}{m!} \frac{d^{m-1}}{d\omega^{m-1}} [A'(\omega)\omega^m] \mathrm{P} \int_0^{\infty} \frac{\{\ln(x)\}^m}{x^2 - 1} dx \tag{34}$$

The integrals in Eq. (34) may be found in many tables of integrals, at least for the first few values of m.[16] For the sake of completeness, however, it will be shown how to evaluate these integrals. The first thing to note is that these integrals vanish for even values of m. This may be seen as follows. Letting $m = 2n$,

$$\mathrm{P} \int_0^{\infty} \frac{(\ln x)^{2n}}{x^2 - 1} dx = \mathrm{P} \int_0^{1} \frac{(\ln x)^{2n}}{x^2 - 1} dx + \mathrm{P} \int_1^{\infty} \frac{(\ln x)^{2n}}{x^2 - 1} dx \tag{35}$$

In the integral from 1 to ∞, making the change of variables $x = \frac{1}{y}$ gives

$$= \mathrm{P}\int_0^1 \frac{(\ln x)^{2n}}{x^2-1}dx + \mathrm{P}\int_1^0 \frac{[\ln(1/y)]^{2n}}{1/y^2-1}d\frac{1}{y} \tag{36}$$

$$= \mathrm{P}\int_0^1 \frac{(\ln x)^{2n}}{x^2-1}dx + \mathrm{P}\int_0^1 \frac{(-\ln y)^{2n}}{1-y^2}dy \tag{37}$$

Now, the minus sign preceding the ln$y$ may be dropped since $2n$ is even. Next writing x in place y gives

$$= \mathrm{P}\int_0^1 \frac{(\ln x)^{2n}}{x^2-1}dx + \mathrm{P}\int_0^1 \frac{(\ln x)^{2n}}{1-x^2}dx = 0 \tag{38}$$

Thus, the sum in Eq. (34) actually ranges over only the odd values of m.

In order to evaluate the remaining integrals, the following contour integral will be used

$$\int_C \frac{(\ln y)^m}{y^2-1}dy = \int_{C_1} \frac{(\ln y)^m}{y^2-1}dy + \int_{C_2} \frac{(\ln y)^m}{y^2-1}dy + \int_{C_3} \frac{(\ln y)^m}{y^2-1}dy \tag{39}$$

$$+ \int_{C_4} \frac{(\ln y)^m}{y^2-1}dy + \int_{C_5} \frac{(\ln y)^m}{y^2-1}dy + \int_{C_6} \frac{(\ln y)^m}{y^2-1}dy = 0$$

where the contour C is that depicted in Fig. (7) together with the subcontours which will be needed below. It must be stressed that the complex plane in which the contour C exists is not the same complex plane as was used to derive the Kramers-Kronig equations. It might be more accurate to refer to the complex plane used in the latter case as the complex angular frequency plane since numbers in that domain have dimensions such as rad-Hz or rad-MHz whereas the complex numbers in which the contour C is placed are dimensionless. In order to differentiate between these two complex planes the convention will be adopted in which dimensionless complex numbers will be denoted by y and the set of these complex numbers referred to as the complex y plane. As a further convention real numbers in the complex y plane will be denoted by the symbol x. Complex numbers in the complex angular frequency plane will be denoted by u and the set of these complex numbers will be referred to as the complex u plane. For example, the expansion of $A(\omega)$ carried out using Burmann's theorem was done in the complex u plane and the integrals appearing as a result of the substitution of this series into the Kramers-Kronig equations have been rescaled, Eq. (27), so that they may be evaluated in the complex y plane. Note that the integral over the large semicircle C_6 vanishes as the radius of that semicircle goes to infinity. Additionally, the integral over the small

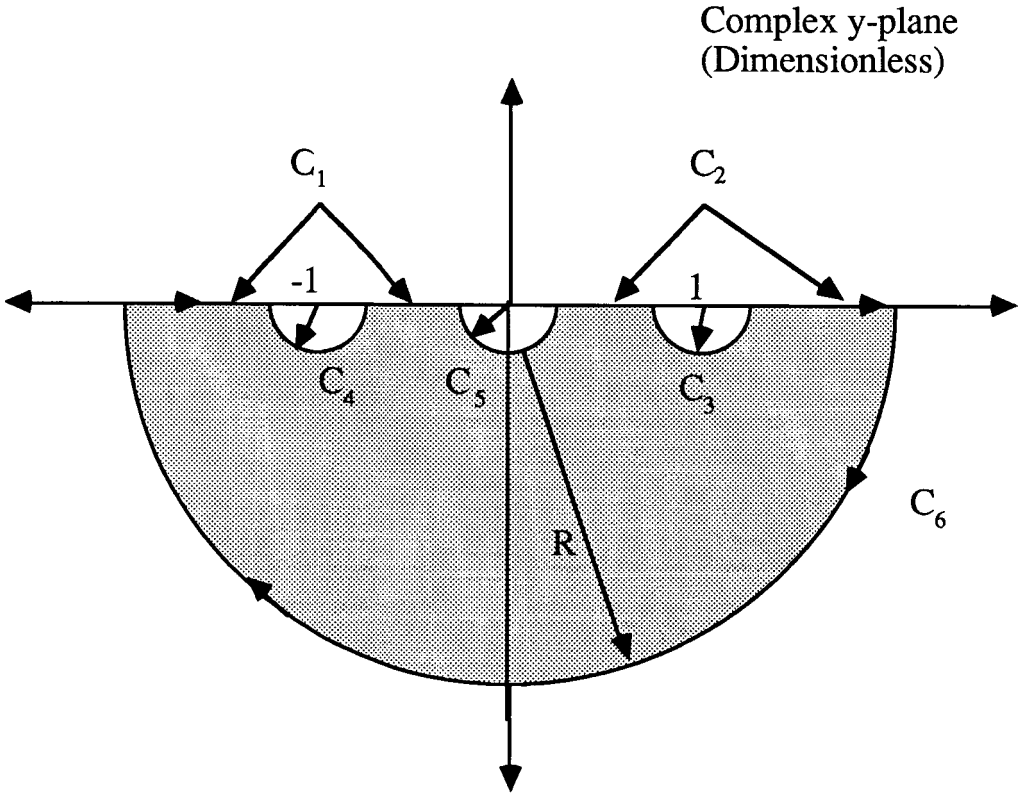

Figure 7). Contour used to evaluate the integrals in Eq.(39) shown in the dimensionless complex y-plane.

semicircle C_5 of radius ρ centered at the origin vanishes as ρ approaches zero. To see this, parameterize the semicircle as follows. Let $y = \rho e^{i\theta}$ where θ ranges from $-\pi$ to π. Then,

$$\int_{C_5} \frac{(\ln y)^m}{y^2-1} dy = \int_{-\pi}^{\pi} \frac{(\ln\rho + i\theta)^m}{\rho^2 e^{2i\theta} - 1} \rho i e^{i\theta} d\theta . \tag{40}$$

Using the binomial theorem permits this to be rewritten as

$$\sum_{k=0}^{m} \binom{m}{k} \rho (\ln\rho)^k \int_{-\pi}^{\pi} \frac{(i\theta)^{m-k} i e^{i\theta}}{\rho^2 e^{2i\theta} - 1} d\theta \tag{41}$$

Furthermore,

$$\lim_{\rho\to 0} \rho(\ln\rho)^k = \lim_{\rho\to 0} \frac{(\ln\rho)^k}{\frac{1}{\rho}} = \lim_{\rho\to 0} \frac{k\frac{1}{\rho}(\ln\rho)^{(k-1)}}{-\frac{1}{\rho^2}} = -k \lim_{\rho\to 0} \frac{(\ln\rho)^{(k-1)}}{\frac{1}{\rho}} \tag{42}$$

where L'Hospital's Rule has been used. We find, after application of this rule k times, that

$$(-1)^{k-1} k! \lim_{\rho\to 0} \rho \ln\rho = 0 \tag{43}$$

So in the limit as $\rho \to 0$ the integral over C_5 vanishes.

We now turn to the evaluation of the contributions from the remaining contours. The integrals over C_4 and C_3 are evaluated using a generalization of the residue theorem. It must be noted, however, that the negative portion of the real axis lies on the second branch of the log function. That is, on the negative real axis,

$$\ln(y) = \ln(|y|) - i\pi \tag{44}$$

Bearing this in mind, we see that the contribution from C_4 is

$$-\pi i \frac{(\ln(1) - i\pi)^m}{2} = \frac{(-i\pi)^{m+1}}{2} \tag{45}$$

(Since $d(y^2-1)/dy$ evaluated at $y = -1$ is -2.) and the contribution from C_3 is

$$\frac{[\ln(1)]^m}{2} = 0 . \tag{46}$$

Now the integrals over C_1 and C_2 may be evaluated as principal value integrals. Collecting results from above gives

$$0 = \int_C \frac{\{\ln y\}^m}{y^2-1} dy = P\int_{-\infty}^{0} \frac{(\ln|x| - i\pi)^m}{x^2-1} dx + P\int_0^{\infty} \frac{(\ln x)^m}{x^2-1} dx + \frac{(-i\pi)^{m+1}}{2} \tag{47}$$

where the convention that real numbers in the complex y plane are to be denoted by x has been used. The binomial theorem may be used to rewrite this as

$$0 = \sum_{k=0}^{m-1}\left[\binom{m}{k}(-i\pi)^{m-k}P\int_0^\infty \frac{(\ln x)^k}{x^2-1}dx\right] + 2P\int_0^\infty \frac{(\ln x)^m}{x^2-1}dx + \frac{(-i\pi)^{m+1}}{2} \tag{48}$$

So

$$P\int_0^\infty \frac{(\ln x)^m}{x^2-1}dx = -\frac{(-i\pi)^{m+1}}{4} - \frac{1}{2}\sum_{k=1}^{m-1}\binom{m}{k}(-i\pi)^{m-k}P\int_0^\infty \frac{(\ln x)^k}{x^2-1}dx \tag{49}$$

For $m = 1$ the sum vanishes and

$$P\int_0^\infty \frac{(\ln x)}{x^2-1}dx = \frac{\pi^2}{4} \tag{50}$$

For $m = 3$ we get

$$P\int_0^\infty \frac{(\ln x)^3}{x^2-1}dx = -\frac{(-i\pi)^4}{4} - \frac{1}{2}\sum_{k=1}^{2}\binom{3}{k}(-i\pi)^{3-k}P\int_0^\infty \frac{(\ln x)^k}{x^2-1}dx \tag{51}$$

$$= -\frac{(-i\pi)^4}{4} - \frac{1}{2}3(-i\pi)^2 P\int_0^\infty \frac{\ln x}{x^2-1}dx$$

$$= -\frac{\pi^4}{4} + \frac{3\pi}{4}\frac{\pi^2}{4}$$

$$= \frac{3\pi^3}{16} - \frac{\pi^4}{2} \tag{52}$$

Thus, from Eq. (34), the local approximation to first order is

$$B(\omega) \approx \frac{2}{\pi}\left[\frac{\pi^2}{4}\right]\left[\omega\frac{dA(\omega)}{d\omega}\right]$$

$$B(\omega) \approx \frac{\pi}{2}\omega\frac{dA(\omega)}{d\omega} \tag{53}$$

To find the corresponding approximation for the other Kramers-Kronig equation, Eq. (11),

$$A(\omega) - A(0) = -\frac{2\omega^2}{\pi}\int_0^\infty \frac{\frac{B(u)}{u} - \frac{B(\omega)}{\omega}}{u^2-\omega^2}du$$

proceed by rewriting it in the following form

$$A(\omega) - A(0) = -\omega\left[\frac{2\omega}{\pi}\int_0^\infty \frac{\frac{B(u)}{u} - \frac{B(\omega)}{\omega}}{u^2-\omega^2}du\right] \tag{54}$$

The expression in the parentheses is identical in form to the integral equation whose approximation has just been derived so long as $B(u)/u$ takes the same role as $A(u)$ took earlier and the expression $A(\omega) - A(0)$ takes the place of $B(\omega)$. Then the following is immediate

$$A(\omega) - A(0) \approx -\frac{\pi\omega^2}{2}\frac{d}{d\omega}\frac{B(\omega)}{\omega} \tag{55}$$

An alternate local approximation may be obtained similarly by starting with Eq. (29) but expanding $A(u)$ in powers of $\ln(-u/\omega)$ about the point $u = \omega$, where the logarithm is thought of as a complex valued function. In this case the same approximation scheme developed above may be used. However, the integrals evaluated in Eq. (34) become

$$\int_0^\infty \frac{\{\ln(-x)\}^m}{x^2-1}dx\ . \tag{56}$$

This is equal to

$$\int_0^\infty \frac{\{\ln(x) - i\pi\}^m}{x^2-1}dx\ . \tag{57}$$

For $m = 1$ this becomes

$$\int_0^\infty \frac{\{\ln(x) - i\pi\}}{x^2-1}dx = \int_0^\infty \frac{\{\ln(x)\}}{x^2-1}dx - i\pi\int_0^\infty \frac{1}{x^2-1}dx \tag{58}$$

$$= \int_0^\infty \frac{\{\ln(x)\}}{x^2-1}dx = \frac{\pi^2}{4}\ .$$

On the other hand, the analog of Eq. (28) is

$$\psi(\omega) = \lim_{u\to\omega}\frac{u-\omega}{\ln\left[-\frac{u}{\omega}\right] - \ln\left[\frac{\omega}{\omega}\right]} = \lim_{u\to\omega} 1/(-1/u) = -\omega\ . \tag{59}$$

This leads to a local approximation which is

$$B(\omega) \approx \frac{2}{\pi}\left[\frac{\pi^2}{4}\right]\left[-\omega\frac{dA(\omega)}{d\omega}\right] = -\frac{\pi}{2}\omega\frac{dA(\omega)}{d\omega}\ . \tag{60}$$

and

$$A(\omega) - A(0) \approx \frac{\pi\omega^2}{2} \frac{d}{d\omega} \frac{B(\omega)}{\omega}$$

This local approximation provides an accurate description of many acoustical systems where the attenuation coefficient is an increasing function of frequency.[17,18]

Before going on, it is worth noting that Burmann's expansion applied directly to $\Theta(\omega)$ could also be used to derive a local approximation. This could be achieved by expanding $\Theta(\omega)$ in terms of some function ϕ chosen to be purely imaginary or real. Taking either the real or imaginary parts of the resulting series expansion would lead to a purely local relation between the real and imaginary parts of $\Theta(\omega)$, i.e., between $A(\omega)$ and $B(\omega)$. However, in this case the right-hand-side of the relation would have terms containing both $A(\omega)$ and $B(\omega)$. The advantage obtained by proceeding as was done in this Section is that the relation obtained gives $A(\omega)$ purely in terms of $B(\omega)$ and *vice versa*.

IIIb. DISCUSSION AND PREVIEW

There is at least one obvious way in which both local approximations may fail. Inspection of Burmann's series, Eq. (26), shows that every term except the first contains $A'(\omega)$. If $A'(\omega)$ happens to be zero then the expansion technique discussed here must fail to give any useful information about the behavior of the function $B(\omega)$. If $A'(\omega) = 0$ then $A(\omega)$ must be a constant. If $A(\omega)$ is constant globally, i.e., constant for all ω, then $B(\omega)$ must be zero also. This result follows from the global form of the Kramers-Kronig equations. However, it is not clear *a priori* that if $A(\omega)$ behaves locally like a constant that $B(\omega)$ must be zero. In this sense the global and local Kramers-Kronig equations lead to the same predictions.

It is also necessary to point out that there is considerable freedom in the choice of the expansion function ϕ used in Burmann's theorem Eq. (25). For example, the function $\ln(-u)$ was used instead of $\ln(u)$ to obtain an alternate local approximation. This led to the local approximation given by Eq. (60). In fact the first local approximation derived, Eq. (53), was tested by Booij and Thoone in viscoelastic theory and found to agree well with experiment. This approximation, Eq. (53), may also have application in acoustics, for instance, in the case where the phase velocity is decreasing with frequency but where the corresponding attenuation must be positive.

It may seem surprising to approximate an integral by a derivative, especially in light of the fact that derivatives usually make functions rougher and integrals usually are considered to be smoothing operators. However, the integrals analyzed in this Section were

singular integrals, so intuition may be misleading in this case. Indeed, the main results of this Section indicates that this is so. In fact, it has been shown in this Section that the Kramers-Kronig integrals behave more like derivatives than regular (i.e., nonsingular) integrals. This result has a precedent in the theory of complex variables in the form of Cauchy's formula for the derivative of an analytic function expressed as a complex contour integral. Beyond that, the local character of these relations should not be surprising when it is recalled that the analysis began with analytic functions. The Cauchy-Riemann equations provide an example of a local relationship between the real and imaginary parts of any function at any point where that function is analytic. Results of a similar nature have been obtained by Widder[19] as well as Paley and Wiener[20] for the case of the Stieltjes transform. Examination of these results should give credibility to the idea that it is possible to obtain local estimates of the behavior of functions related by nonlocal integral equations.

Specifically, the Stieltjes transform of $\phi(t)$ is

$$f(x) = \int_0^\infty \frac{\phi(t)}{x+t} dt \ .$$

Widder has shown that this nonlocal relation has the purely local inversion given by

$$\phi(t) = \lim_{k \to \infty} \frac{(-t)^{k-1}}{k!(k-2)!} \frac{d^{k-1}}{dt^{k-1}} [t^k f(t)] \ .$$

Paley and Wiener derive an alternate local expression which is

$$\phi(t) = \lim_{m \to \infty} \frac{1}{\pi t^{1/2}} \sum_0^m (-1)^n \frac{\left[\pi t \frac{d}{dt}\right]^{2n}}{(2n)!} (t^{1/2} f(t)) \ .$$

A common feature to both of these expressions is that they call for the evaluation of derivatives up to infinite order. This seems to be a common feature of many local inversion formulae of nonlocal operators.

IIIc. THE LOCAL APPROXIMATION IN ACOUSTICS

In this Section the local approximations derived in Section IIIa. will be applied to acoustical systems. In Section IIIb.1 we will derive a local approximation relating dispersion to attenuation in systems exhibiting small dispersion. In Section IIIc.2 we will generalize this relation to systems in which the dispersion is not necessarily small. Thus, we will fulfill one of the objectives of our previous proposal which was to generalize these relations to systems which exhibit considerable dispersion. In this Section we shall also see that the acoustic index of refraction could have been chosen as our frequency response function without changing any of our results. Thus our approach and that taken other researchers, who used the acoustic index of refraction for their frequency response function, are essentially equivalent. A preview of the results that we will obtain in this Section is presented in Table 1.

1) The Case of Small Dispersion

Up to now everything that has been done is perfectly general. At this point a specific frequency response function $\Theta(\omega)$ will be chosen, namely, the dynamic compressibility $K(\omega)$ of the medium in which a traveling sound wave will be propagated. (In this Section of the report we will apply the local approximation, Eq. (60) to weakly dispersive materials. This is essentially a review of previously reported results and is included to provide a contrast with the material to be presented in Section IIIc.2 of the present report.) At this point the attenuation coefficient and phase velocity finally enter. This is because the frequency dependent compressibility must also satisfy the dispersion relation for acoustic wave propagation,

$$k^2 = \omega^2 \rho_0 K(\omega) , \tag{61}$$

where k is the wave number of the acoustic wave, and ρ_0 is the density of the material. Making the usual identification that

$$k = \frac{\omega}{C(\omega)} + i\,\alpha(\omega) \tag{62}$$

where $C(\omega)$ is the phase velocity of the acoustic wave and $\alpha(\omega)$ is the attenuation coefficient, and substituting this relation into Eq. (61) gives

$$\left[\frac{\omega}{C(\omega)} + i\,\alpha(\omega) \right]^2 = \omega^2 \rho_0 K(\omega) . \tag{63}$$

Writing $K(\omega)$ as the sum of its real and imaginary parts,

$$K(\omega) = K_1(\omega) + iK_2(\omega) , \tag{64}$$

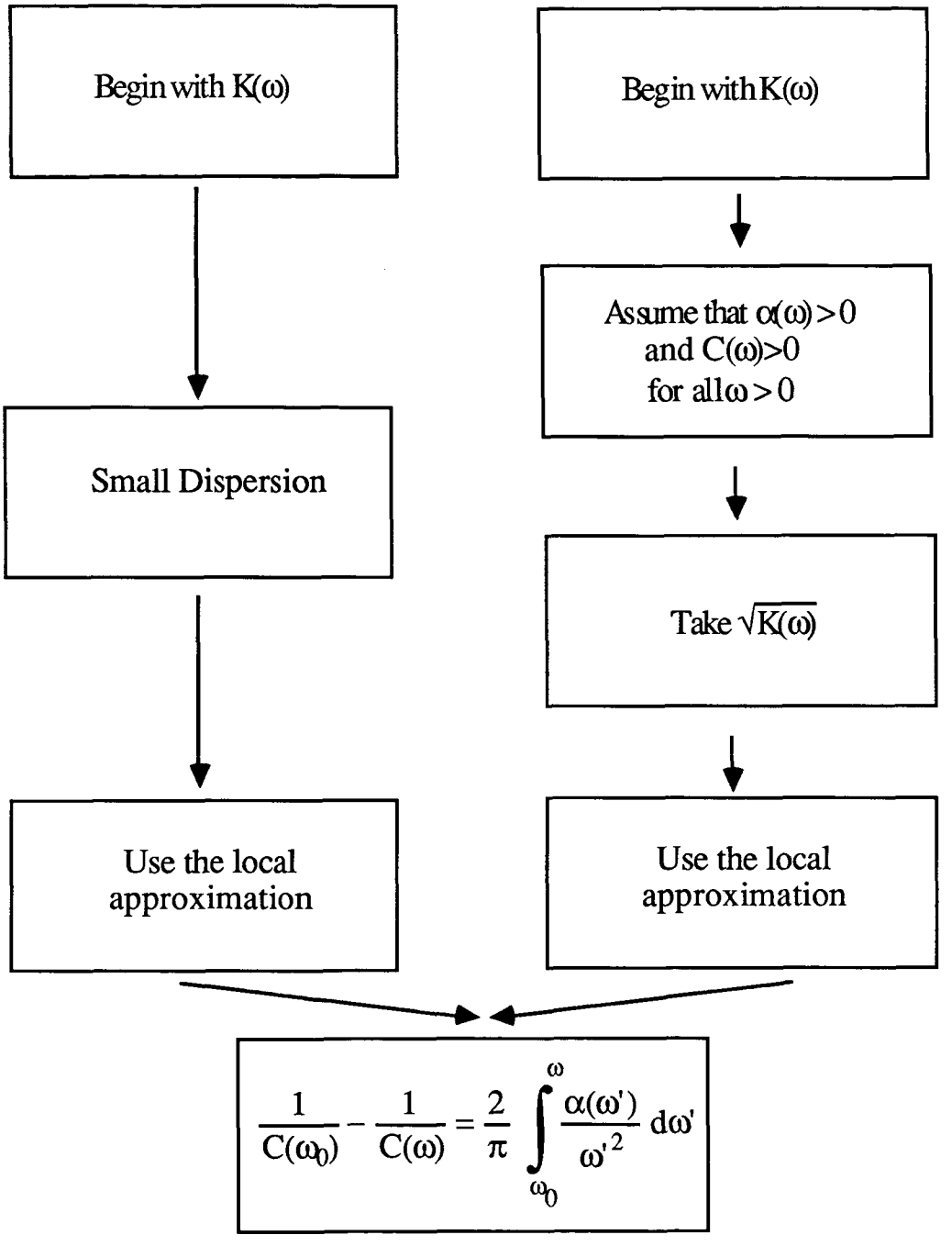

Table 1. A flow chart showing the different developments given in Section IIIc.1 (shown in the left column) and IIIc.2 (shown in the right column). Both developments lead to the same conclusion but the path on the right is more general.

inserting this into Eq. (63), and equating real and imaginary parts gives

$$\left[\frac{\omega}{C(\omega)}\right]^2 - \alpha^2(\omega) = \omega^2\rho_0 K_1(\omega) \tag{65}$$

$$\frac{2\alpha(\omega)}{C(\omega)} = \omega\rho_0 K_2(\omega) \tag{66}$$

Shortly, $K_1(\omega)$ will be identified with $A(\omega)$ and $K_2(\omega)$ will be identified with $B(\omega)$. However, before this can be done, Eqs. (65) and (66) must be decoupled in order to simplify the derivation below. This may be accomplished via the following approximation

$$\frac{\alpha(\omega)C(\omega)}{\omega} \ll 1 \tag{67}$$

which is true in many experimental situations. Eq. (67) states that the magnitude of the imaginary part of the wave vector is much less than the magnitude of the real part. Table 2 contains a compilation of typical values for the left-hand side of Eq. (67). The Table is organized in terms of increasing values of a parameter β, the so-called slope of attenuation which is defined in Eq. (82). We note that Eq. (67) is very well satisfied for all entries in Table 2. With this assumption Eqs. (65) and (66) become

$$\rho_0 K_1(\omega) = \left[\frac{1}{C(\omega)}\right]^2 - \frac{\alpha^2(\omega)}{\omega^2} \tag{68}$$

$$\rho_0 K_2(\omega) = \left[\frac{2\alpha(\omega)}{\omega}\right]\left[\frac{1}{C(\omega)}\right].$$

Dropping the small term gives

$$\rho_0 K_1(\omega) \approx \left[\frac{1}{C(\omega)}\right]^2 \tag{69}$$

$$\rho_0 K_2(\omega) = \left[\frac{2\alpha(\omega)}{\omega}\right]\left[\frac{1}{C(\omega)}\right].$$

These equations may now be solved for $K_1(\omega)$ and $K_2(\omega)$, yielding

$$K_1(\omega) \approx \frac{1}{\rho_0 C(\omega)^2} \tag{70}$$

$$K_2(\omega) = \frac{2\alpha(\omega)}{\rho_0 \omega C(\omega)} \tag{71}$$

Now Eq. (60) may be applied to obtain

$$K_2(\omega) \approx -\frac{\pi}{2}\omega\frac{dK_1(\omega)}{d\omega} \tag{72}$$

Material	Slope of Attenuation		Att. Coeff.	Phase Vel .	Coupling Term
	β (dB/MHz–cm)	β (1/MHz–m)	α (1/m) at 5MHz	C (m/sec) at 5 MHz	$\alpha(f)C(f)/2\pi f$ at 5MHz
Styrene @ 28°c	0.3	3.3	16.5	2295	1.2×10^{-3}
Lucite @ 28°c	1.1	12.7	63.5	2680	5.4×10^{-3}
Lucite @ 54°c	1.7	18.1	94	2690	8.0×10^{-3}
Epoxy @ 28°c	4.3	47.5	237.5	2400	1.8×10^{-2}
Lexan @ 54°c	4.9	54.1	270.5	2222	1.9×10^{-2}
Lexan @ 28°c	5.0	55.3	276.5	2196	1.9×10^{-2}
Polyethylene @ 28°c	6.2	68.5	342.5	2000	2.2×10^{-2}
Epoxy @ 54°c	6.5	71.8	359	2400	2.7×10^{-2}

Table 2. A compilation of the ultrasonic parameters needed to compute the coupling term appearing in Eq.(162). The materials tabulated above cover a 20 to 1 variation in the value of the slope of attenuation, beta. The value of f was chosen to be 5 MHz for the computed values shown for the coupling term presented in the right-most column.

Substituting the expression for $K_1(\omega)$ in terms of $C(\omega)$ gives the following expression for $dK_1(\omega)/d\omega$

$$\frac{dK_1(\omega)}{d\omega} \approx -\frac{1}{\rho_0}\frac{-2}{C(\omega)^3}\frac{dC(\omega)}{d\omega} \tag{73}$$

$$\frac{dC(\omega)}{d\omega} \approx \frac{\rho_0 C(\omega)^3}{2}\frac{dK_1(\omega)}{d\omega} \tag{74}$$

Now substituting Eq. (74) into Eq. (72) gives

$$\frac{dC(\omega)}{d\omega} \approx \frac{\rho_0 C(\omega)^3}{2}\frac{2}{\pi}\frac{1}{\omega}K_2(\omega)\,. \tag{75}$$

The expression for $K_2(\omega)$ in terms of $\alpha(\omega)$ may be used to obtain

$$\frac{dC(\omega)}{d\omega} \approx \frac{2C(\omega)^2\alpha(\omega)}{\pi\omega^2}\,, \tag{76}$$

from Eq. (75). This equation, Eq. (76), may be rewritten as a separable differential equation,

$$\alpha(\omega) \approx \frac{\pi\omega^2}{2C(\omega)^2}\frac{dC(\omega)}{d\omega} \tag{77}$$

which may be solved by integration. This leads to

$$\frac{2}{\pi}\int_{\omega_0}^{\omega}\frac{\alpha(\omega')}{\omega'^2}d\omega' \approx \int_{\omega_0}^{\omega}\frac{dC(\omega')}{C(\omega')^2} = \frac{1}{C(\omega_0)} - \frac{1}{C(\omega)} \tag{78}$$

It is worth noting that the approximation in Eq. (67) was essential to the derivation of this equation. It will be seen later that there is another way to derive Eq. (78) which rests solely on the local approximation and which is not limited by the assumption of small dispersion. However, at this point it is again necessary to use the fact that the material has small dispersion, that is,

$$C(\omega_0) \approx C(\omega)\,. \tag{79}$$

Then it is found that

$$\frac{1}{C(\omega_0)} - \frac{1}{C(\omega)} = \frac{C(\omega) - C(\omega_0)}{C(\omega_0)C(\omega)} \approx \frac{C(\omega) - C(\omega_0)}{C(\omega_0)^2} \tag{80}$$

This leads finally, with $C_0 \equiv C(\omega_0)$, to

$$C(\omega) - C_0 = \frac{2C_0^2}{\pi}\int_{\omega_0}^{\omega}\frac{\alpha(\omega')}{\omega'^2}d\omega'\,. \tag{81}$$

As we have reported in previous progress reports this equation agrees well with experimental data, obtained from both homogeneous and inhomogeneous materials, for frequencies from 2 MHz to 20 MHz. However, it may hold over a much wider frequency range. Table 3 presents the predictions of Eq. (81) for a variety of different dependences of the attenuation coefficient on frequency. In certain cases further conclusions may be drawn from Eq. (81). For instance, experimental evidence indicates that the attenuation is an approximately linear function of frequency for a wide range of frequencies, i.e.,

$$\alpha(\omega) = \frac{\beta}{2\pi}\omega \tag{82}$$

for a wide range of materials. With this assumption, Eq. (81) predicts

$$C(\omega) - C_0 \approx \frac{C_0^2 \beta}{\pi^2}\ln(\omega/\omega_0)\,. \tag{83}$$

III2) Acoustical Systems where the Dispersion Is Not Necessarily Small

As mentioned above, it is not really necessary to make the assumption that the dispersive effects are small. This may be accomplished by, first, showing that $K(\omega) \neq 0$ in the lower half plane, which permits the square root of Eq. (63) to be taken without introducing any singularities in the lower half plane. This procedure produces a new system response function, also analytic in the lower half plane, which has real and imaginary parts that are functions of $\alpha(\omega)$ and $C(\omega)$. The resulting Kramers-Kronig relations, obtained for this new system response function, are the same as those obtained by researchers who use the acoustic index of refraction for their frequency response function. Before this can be demonstrated, however, a small detour into the theory of complex variables must be made. The development given here follows closely that given by Landau and Lifshitz.[21] It rests on two theorems from complex variables which for completeness will be stated here. For convenience they will be called Theorem 2 and Theorem 3. They are:

Theorem 2:

Let a function f be analytic inside and on a simple closed contour C, except for at most a finite number of poles interior to C. Additionally, let f have no zeros on C and at most a finite number of zeros interior to C. Then if C is described in the positive sense,

$$\frac{1}{2\pi i}\int_C \frac{f'(z)}{f(z)}dz = N - P \tag{84}$$

Description	Observed Frequency Dependence of Attenuation Coefficient	Predicted Frequency Dependence of Phase Velocity
Rayleigh Scattering	ω^4	ω^3
Classical Viscous	ω^2	ω^1
Plastics, Composites Soft Tissue	ω^1	$\ln \omega$
Geometric Scattering (Hollow Pores)	ω^0	ω^{-1}

Table 3. A compilation of the observed behavior of the frequency dependence of the attenuation ceofficient for several physical phenomena and the corresponding frequency dependence of the phase velocity as predicted by Eq.(81).

where N is total number of zeros of f inside C and P is the total number of poles there. A zero of order m_0 is to be counted m_0 times, and a pole of order m_p is to be counted m_p times.

The next theorem is known as the Argument Principle.

Theorem 3:

Let C be a simple closed contour described in the positive sense and let f be a function which is analytic inside and on C, except possibly for poles interior to C. Additionally, let f have no zeros on C. Then

$$\frac{1}{2\pi}\Delta_C \arg f(z) = N - P \tag{85}$$

where N and P are the number of zeros and the number of poles of f, counting multiplicities, interior to C and $\Delta_C \arg f(z)$ is the change in the argument of f as we traverse the contour C once.

If we now return to the very general setting in which the Kramers-Kronig integral equations were established, and, furthermore, if we suppose that $\Theta(\omega)$ is such that its imaginary part $B(\omega)$ is never zero on the real ω axis except at zero and infinity, we will be able show that $\Theta(\omega)$ has no zeros in the lower half of the complex ω plane.

Our first step is to consider the integral

$$\frac{1}{2\pi i}\int_C \frac{d\Theta(\omega)}{d\omega}\frac{d\omega}{\Theta(\omega)-a} \tag{86}$$

where C is the contour shown in Fig. (8). According to Theorem 2 this is equal to the difference between the number of zeros and the number of poles of the function $\Theta(\omega)-a$ in the region interior to the contour C. Let a be a real number and C be the contour consisting of the real axis and an infinite semicircle in the lower half plane. Suppose that $\Theta(0) \equiv \Theta_0$ is finite. Since $\Theta(\omega)$ is analytic in the lower half plane, so is $\Theta(\omega)-a$. Therefore the integral in Eq. (86) is simply the number of zeros of the function $\Theta(\omega)-a$, that is, the number of points at which $\Theta(\omega)$ takes on the real value a. Our next step is to perform the conformal mapping from the ω plane to the Θ plane via the transformation

$$\omega \rightarrow \Theta, \quad \Theta = \Theta(\omega). \tag{87}$$

Under this transformation Eq. (86) becomes

$$\frac{1}{2\pi i}\int_{C'}\frac{d\Theta}{\Theta-a} \tag{88}$$

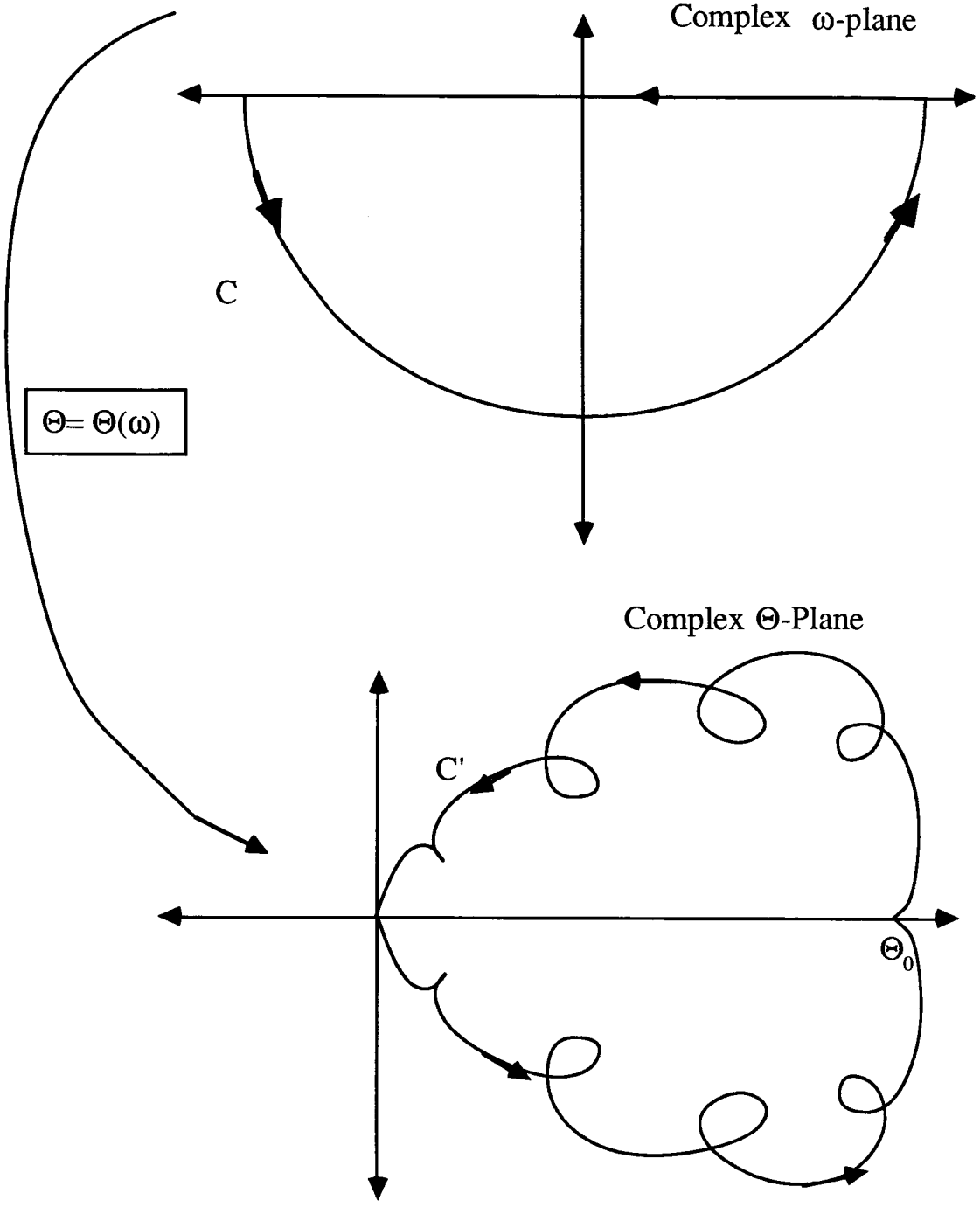

Figure 8). Drawing of the contour used in Eq.(86) and its image under the conformal transformation defined in Eq.(87).

The contour C' is the image of the contour C under the conformal transformation defined in Eq. (87). C' is depicted schematically in Fig. (8). Now, the function $\Theta(\omega)$ goes to zero as ω goes to ∞ by the Riemann-Lesbegue Lemma. For this reason the entire infinite semicircle in the contour C is mapped onto the single point $\Theta = 0$ on C'. The point $\omega = 0$ is mapped onto the point $\Theta = \Theta_0$. Furthermore, Θ_0 is real since $\Theta_0 \equiv \Theta(0) = A(\omega)$ (since $B(\omega) = 0$ when $\omega = 0$). The right and left halves of the real ω axis are mapped onto some very complicated (and generally self-intersecting) curves whose shape is not significant. The important thing about these curves is that they lie entirely in the upper and lower halves of the Θ plane respectively. This observation about the image of the positive ω axis follows from the assumption that the imaginary part $B(\omega)$ of $\Theta(\omega)$ is strictly greater than zero, except at $\omega = 0$ or ∞. The corresponding result for the image of the negative ω axis follows immediately then from the odd parity of the function $B(\omega)$. Since $B(\omega)$ is strictly greater than zero, the two images in the complex Θ plane nowhere intersect the real axis of the complex Θ plane. Because of this property of the curve C', it can be seen that the total change in the argument of the complex number $\Theta - a$, as we pass once around the contour C', is 2π if a lies between 0 and Θ_0 or zero if a lies outside that range. Hence it follows from Theorem 3 that the expression in Eq. (88) is unity for $0 < a < \Theta_0$, and zero otherwise.

Thus we conclude that, if a is in this range, then $\Theta(\omega)-a$ takes the value zero once and only once for ω in the lower half plane, but if not, then $\Theta-a$ is never zero in the lower half plane. Hence, we deduce that on the negative imaginary ω axis, where the function $\Theta(\omega)$ is real, it cannot have either a maximum or a minimum since otherwise it would take on some values at least twice. As a result $\Theta(\omega)$ varies monotonically on the negative imaginary ω axis. Because Θ is analytic in the lower half plane, it can be seen that on the negative imaginary axis, and nowhere else, Θ takes on all real values between 0 and Θ_0 once and only once.

Let's now return to our previous setting, and replace $\Theta(\omega)$ by $K(\omega)$. We observe that the imaginary part of $K(\omega)$ is

$$\frac{2\alpha(\omega)}{C(\omega)} = \omega\rho_0 K_2(\omega) \tag{89}$$

Physically, it is clear that $C(\omega)$ and $\alpha(\omega)$ are never less than or equal to zero for any positive value of ω. Thus we see that $K_2(\omega) > 0$ for all positive ω. This means that $K(\omega)$ is never zero in the lower half ω plane and, as has already been shown, that it is analytic there. Thus the square root of $K(\omega)$ must be analytic in the lower half of the ω plane. Hence, by Eqs. (63) and (64) the physical quantity $\frac{1}{\sqrt{\rho_0}}\frac{1}{C(\omega)}$ is the real part of

a Kramers-Kronig pair and that $\frac{1}{\sqrt{\rho_0}}\frac{\alpha(\omega)}{\omega}$ is its corresponding imaginary part. Inserting these quantities into the local approximation, Eq. (60), and canceling the factor of $\frac{1}{\sqrt{\rho_0}}$ that appears on both sides of the resulting equation yields

$$\frac{\alpha(\omega)}{\omega} \approx -\frac{\pi}{2}\omega\frac{d}{d\omega}\frac{1}{C(\omega)} \tag{90}$$

which leads to

$$\frac{2}{\pi}\int_{\omega_0}^{\omega}\frac{\alpha(\omega')}{\omega'^2}d\omega' \approx \frac{1}{C(\omega_0)} - \frac{1}{C(\omega)} \tag{91}$$

This is precisely the same result that was obtained earlier in Eq. (78) by assuming that dispersive effects were small. However, this restriction appears nowhere in the derivation of Eq. (91). Thus, the local approximation, Eq. (91), may hold in systems which exhibit considerable dispersion such as carbon-carbon composites. Table 1 reviews the developments given in Sections III.c.1 and III.c.2.

References

1. J. H. Rose, D. K. Hsu, and L. Adler, "Ultrasonic characterization of porosity using the Kramers-Kronig relations," *Journal De Physique*, vol. 46, pp. 787-790, 1985.
2. J.E. Gubernatis, E. Domany, J.A. Krumhansl, and M. Huberman, *The Fundamental Theory of Elastic Wave Scattering by Defects in Elastic Materials: Integral Equation Methods for Application to Ultrasonic Flaw Detection,* Materials Science Center, Cornell University, Technical Report 2654, Ithaca, NY, 1976. Unpublished.
3. L. Adler, J. H. Rose, and C. Mobley, "Ultrasonic method to determine gas porosity in aluminum alloy castings: theory and experiment," *J. Appl. Phys.*, vol. 59, pp. 336-347, 1986.
4. S. M. Nair, "Quantitative evaluation of porosity in graphite-epoxy composites using the frequency dependence of ultrasonic attenuation," *Masters Thesis (Iowa State University, Ames, Iowa)*, 1986 .
5. B. R. Tittmann, B. Hosten, and M.Abdel-Gawad, "Ultrasonic attenuation in carbon-carbon composites and the determination of porosity," *Proceedings of the 1986 IEEE Ultrasonics Symposium CH2375-4*, pp. 1047-1049, 1986.
6. D. K. Hsu and S. M. Nair, "Evaluation of porosity in graphite-epoxy composite by frequency dependence of ultrasonic attenuation," in *Review of Progress in Quantitative NDE*, ed. D. O. Thompson & D. E. Chimenti, vol. 6B, pp. 1185-1193, Plenum

Press, New York, 1986.

7. S. M. Nair, D. K. Hsu, and J. H. Rose, "Ultrasonic characterization of cylindrical porosity - A model study," in *Review of Progress in Quantitative NDE*, ed. D. O. Thompson & D. E. Chimenti, vol. 6B, pp. 1165-1174, Plenum Press, New York, 1986.
8. D. K. Hsu and K. M. Uhl, "A morphological study of porosity defects in graphite-epoxy composites," in *Review of Progress in Quantitative NDE*, ed. D. O. Thompson & D. E. Chimenti, vol. 6B, pp. 1175-1184, Plenum Press, New York, 1986.
9. M. D. Fuller and P. M. Gammel, "Ultrasonic characterization of porosity in composite materials by time delay spectroscopy," in *Review of Progress in Quantitative NDE*, ed. D. O. Thompson & D. E. Chimenti, vol. 6B, pp. 1157-1163, Plenum Press, New York, 1986.
10. S. M. Nair, D. K. Hsu, and J. H. Rose, *Characterization of cylindrical pores using ultrasonic attenuation*, to be published in J. Appl. Phys..
11. J. Ophir, T.H. Shawker, N.F. Maklad, J.G. Miller, S.W. Flax, P.A. Narayana, and J.P. Jones, "Attenuation Estimation in Reflection: Progress and Prospects," *Ultrasonic Imaging*, vol. 6, pp. 349-395, 1984.
12. J. H. Rose, "Kramers-Kronig relations and the ultrasonic characterization of porosity," in *Review of Progress in Quantitative NDE*, ed. D. O. Thompson & D. E. Chimenti, vol. 5, Plenum Press, New York, 1985.
13. *Tables of Integral Transforms*, pp. 243-253, McGraw Hill, New York, 1954.
14. F.G. Tricomi, *Integral Equations*, p. 169, Dover Publications, New York, 1957.
15. E. T. Whittaker and G. N. Watson, *A Course of Modern Analysis*, Cambridge University Press, London, 1927.
16. I. S. Gradshteyn and I. M. Ryzhik, *Table of Integrals, Series, and, Products*, Academic Press, New York, 1980.
17. M. O'Donnell, E.T. Jaynes, and J.G. Miller, "General Relationships Between Ultrasonic Attenuation and Dispersion," *J. Acoust. Soc. Am.*, vol. 63, pp. 1935-1937, 1978.
18. M. O'Donnell, E.T. Jaynes, and J.G. Miller, "Kramers-Kronig Relationship Between Ultrasonic Attenuation and Phase Velocity," *J. Acoust. Soc. Am.*, vol. 69, pp. 696-701, 1981.
19. D. V. Widder, *The Laplace Transform and its Applications*, pp. 277-391, Princeton University Press, Princeton, N.J., 1946.
20. R. E. A. C. Payley and N. Wiener, *Fourier Transforms in the Complex Plane*, 19, p. 43, American Mathematical Society, Providence, R.I., 1934.

21. L. D. Landau and E. M. Lifshitz, *Statistical Physics,* p. 380, Pergamon Press, London, 1958.